


## The OSIRIS-REx Laser Altimeter (OLA) Investigation and Instrument

M.G. Daly<sup>1</sup>  · O.S. Barnouin<sup>2</sup> · C. Dickinson<sup>3</sup> · J. Seabrook<sup>1</sup> · C.L. Johnson<sup>4</sup> · G. Cunningham<sup>5</sup> · T. Haltigin<sup>6</sup> · D. Gaudreau<sup>6</sup> · C. Brunet<sup>6</sup> · I. Aslam<sup>3</sup> · A. Taylor<sup>3</sup> · E.B. Bierhaus<sup>7</sup> · W. Boynton<sup>8</sup> · M. Nolan<sup>8</sup> · D.S. Lauretta<sup>8</sup>

Received: 20 January 2017 / Accepted: 3 May 2017 / Published online: 1 August 2017  
© Springer Science+Business Media Dordrecht 2017

**Abstract** The Canadian Space Agency (CSA) has contributed to the Origins Spectral Interpretation Resource Identification Security-Regolith Explorer (OSIRIS-REx) spacecraft the OSIRIS-REx Laser Altimeter (OLA). The OSIRIS-REx mission will sample asteroid 101955 Benu, the first B-type asteroid to be visited by a spacecraft. Benu is thought to be primitive, carbonaceous, and spectrally most closely related to CI and/or CM meteorites. As a scanning laser altimeter, the OLA instrument will measure the range between the OSIRIS-REx spacecraft and the surface of Benu to produce digital terrain maps of unprecedented spatial scales for a planetary mission. The digital terrain maps produced will measure  $\sim 7$  cm per pixel globally, and  $\sim 3$  cm per pixel at specific sample sites. In addition, OLA data will be used to constrain and refine the spacecraft trajectories. Global maps and highly accurate spacecraft trajectory estimates are critical to infer the internal structure of the asteroid. The global and regional maps also are key to gain new insights into the surface processes acting across Benu, which inform the selection of the OSIRIS-REx sample site. These, in turn, are essential for understanding the provenance of the regolith sample collected by the OSIRIS-REx spacecraft. The OLA data also are important for quantifying any hazards near the selected OSIRIS-REx sample site and for evaluating the range of tilts at the sampling site for comparison against the capabilities of the sample acquisition device.

---

OSIRIS-REx

Edited by Dante Lauretta and Christopher T. Russell

---

✉ M.G. Daly  
[dalym@yorku.ca](mailto:dalym@yorku.ca)

<sup>1</sup> Centre for Research in Earth and Space Science, York University, Toronto, Ontario, Canada

<sup>2</sup> Johns Hopkins University Applied Physics Laboratory, Laurel, MD, USA

<sup>3</sup> MDA, Brampton, Ontario, Canada

<sup>4</sup> University of British Columbia, Vancouver, British Columbia, Canada

<sup>5</sup> Teledyne Optech, Vaughn, Ontario, Canada

<sup>6</sup> Canadian Space Agency, St. Hubert, Quebec, Canada

<sup>7</sup> Lockheed Martin, Denver, CO, USA

<sup>8</sup> University of Arizona, Tucson, AZ, USA

**Keywords** Asteroid · Lidar · Altimeter · OSIRIS-REx · Bennu

### Abbreviations

APD	avalanche photodiode
CAT	category
CCA	circuit card assembly
CFD	constant-fraction discriminator
CSA	Canadian Space Agency
EMC	electromagnetic compatibility
HELT	high-energy laser transmitter
LELT	low-energy laser transmitter
LVDS	low voltage differential signalling
MDA	MacDonald, Dettwiler and Associates
OAP	off-axis parabolic mirror
OCAMS	OSIRIS-REx Camera Suite
OLA	OSIRIS-REx Laser Altimeter
OSIRIS-REx	Origins, Spectral Interpretation, Resource Identification, and Security-Regolith Explorer
OTES	OSIRIS-REx Thermal Emission Spectrometer
OVIRS	OSIRIS-REx Visible and Infrared Spectrometer
POST	Power-On Self-Test
REXIS	Regolith X-ray Imaging Spectrometer
SBC	single-board computer
SCLK	spacecraft clock
TIM	Time-Interval Meter

## 1 Introduction

### 1.1 Mission Overview and the Role of OLA

The objective of Origins, Spectral Interpretation, Resource Identification and Security-Regolith Explorer (OSIRIS-REx) is to return a sample from asteroid 101955 Bennu (Lauretta et al. 2017). The instruments aboard the OSIRIS-REx spacecraft will measure the properties of the asteroid to support the investigation of the geophysical and geochemical state of this B-class asteroid, a subclass within the larger group of C-complex asteroids, that might be organic-rich. At approximately 500 m in average diameter (Nolan et al. 2013), Bennu is large enough to retain substantial regolith and as an Apollo asteroid with a low inclination ( $6^\circ$ ), Bennu is the most accessible primitive near-Earth asteroid (Lauretta et al. 2015).

The OSIRIS-REx spacecraft, launched in September 2016, will rendezvous with asteroid 101955 Bennu in mid-2018. It will ultimately return samples of the asteroid back to the Earth, the first US mission to do so. The returned samples may hold clues to the origin of the solar system and possible organic molecules that may have seeded life on Earth.

As part of a suite of instruments on the OSIRIS-REx spacecraft, the OSIRIS-REx Laser Altimeter (OLA) is the world's first scanning laser rangefinder (or lidar) to fly on a planetary mission. Other instruments that make up the scientific payload include cameras (OCAMS) (Rizk 2017), a visible and near-infrared spectrometer (OVIRS) (Reuter et al. 2017), a thermal emission spectrometer (OTES) (Christensen et al. 2017), and an X-ray imaging spectrometer (REXIS) (Binzel 2017).

The OLA instrument is very flexible in its ability to collect data because of its long- and short-range laser transmitters and its scanning mirror. This flexibility is ideal for continuously improving the fidelity of topographical products generated by OLA during the different phases of the OSIRIS-REx mission, as the spacecraft slowly approaches and eventually touches the asteroid. OLA has a series of scientific and mission objectives that can be divided into global and sample-site-scale investigations.

At a global scale, OLA will measure the shape of Bennu to provide insights into the geological origin and evolution of the asteroid by, for example, constraining its bulk density through precise volume measurement. Combined with a carefully undertaken geodesy campaign (McMahon et al. 2017), OLA-based precision ranges, radio science (two-way tracking) data and stereo OCAMS images will yield constraints on any global-scale internal heterogeneity of Bennu and hence provide further clues to its origin and subsequent collisional evolution. The OLA-derived asteroid shape, when combined with a mass or gravity measurement, will provide global maps of slopes, geopotential elevation or altitude relative to the asteroid geoid (Scheeres et al. 2016), and vertical roughness that will provide quantitative insights (Cheng et al. 2001; Barnouin-Jha et al. 2008) into how the surface of Bennu evolved subsequent to the formation of the asteroid. Establishing any connection between surface morphological features that possess measurable topography and their spatial relationships to other geological features, such as craters, will provide additional constraints on the interior structure and geophysical evolution of Bennu (Marchi et al. 2015).

Over the sample-site ( $\sim 50$  m diameter), OLA will provide detailed information on the geological and geophysical processes that influence the surface regolith at scales ( $\sim 5$  cm and greater) relevant to the samples that will be collected. High resolution (centimeter-scale) spatial measurements of surface topographic slopes, center of mass-referenced elevation, and vertical roughness within the sample ellipse will provide data on processes such as surface granular flows (Miyamoto et al. 2007) that have influenced the regolith distribution on the asteroid. This has implications for the selection of the OSIRIS-REx sample site. OLA data will also be used to assess hazards and sampleability at any proposed sample site. Specifically, OLA will provide data that will allow the team to measure the geopotential slope and tilt distribution within the sample ellipse and characterize backscatter roughness at or below the scale of the OLA spot size.

OLA also serves the function of a basic ranging device by providing precision ranges that are used as a part of the data input to the navigation solutions. These fundamental measurements provide increased confidence and faster navigation timelines, thereby improving efficiency, accuracy and overall mission safety. Additionally, the range measurements also allow other instrument teams to improve the scaling of their images or spectral sampling.

## 1.2 OLA Instrument Overview

The Canadian Space Agency (CSA) contributed OLA to OSIRIS-REx. The instrument was built for the CSA by Canadian firm MacDonald, Dettwiler and Associates (MDA), with lidar sensors designed and provided by subcontractor Teledyne Optech, based in Vaughan, Ontario. The OLA science team is led by York University with support from the University of British Columbia and our United States-based partners.

OLA was developed using heritage components and approaches from previous space-flight missions. The scanning system and low-energy transmitter share heritage with the lidar used aboard the experimental XSS-11 mission (Nimelman et al. 2005). The high-energy laser is a modified version of that used in the meteorology lidar on the Phoenix Mars Mission (Whiteway et al. 2008).

**Table 1** OLA was developed to the following summary set of technical specifications, provided for the High and Low Energy Transmitters as appropriate. Specifications are based on performance to a 3% Lambertian reflector

Specification	High energy	Low energy
Maximum operational range	> 7.4 km	> 0.75 km
Minimum operational range	< 1.0 km	< 0.475 km (< 200 m goal)
Range accuracy ( $1\sigma$ )	< 0.5 m	< 0.3 m
Range precision ( $1\sigma$ )	< 0.3 m	< 0.04 m
Scanner field of regard	$\pm 10^\circ$ (azimuth), $\pm 6^\circ$ (elevation)	
Scanner precision	< 100 $\mu$ rad	< 100 $\mu$ rad
Laser divergence ( $1/e$ )	200 $\mu$ rad	100 $\mu$ rad

These heritage items were used to constrain the conceptual design in order to reduce development risk. Additional constraints were taken from the mission concept of operations discussed in Sect. 2.1 and in more detail in Lauretta et al. (2017). From these constraints, we developed a set of specifications for the OLA instrument (Table 1). The initial concept was a two-box design with optics, lasers, and detectors in one enclosure, and the main electronics in a second one. This approach provided flexibility in accommodating the instrument on the spacecraft.

The maximum required operational range of OLA of  $\sim 7$  km from the asteroid combined with the 1 mJ-class Phoenix laser pulse energy and the sensitivity of the XSS-11-derived constant-fraction receiver set the receiver aperture at  $\sim 75$  mm with a 3 dB link margin. The power-aperture product of the low energy laser provided a 750 m operational range, also with a 3 dB link margin. To achieve global coverage of Bennu and to make efficient use of the 10 kHz maximum measurement rate of OLA, a scanning mirror is required. To understand the importance of this system, it should be noted that the ground-track velocity of the spacecraft is of the same order as one spot diameter per second. Therefore, without an OLA scanning capability, thousands of measurements per second would not be efficiently placed. Spacecraft slewing could improve the situation, but most of the high measurement-rate capability would not be effective.

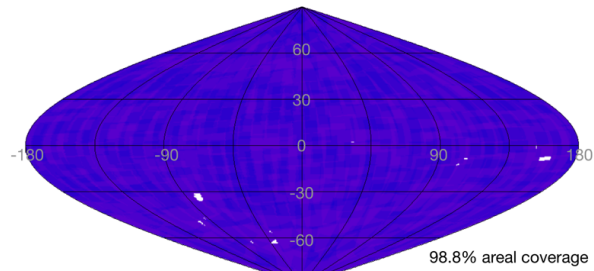
### 1.3 Comparison with Previous Planetary Lidars

Table 2 presents a comparative suite of planetary lidars. OLA differs from many of these lidars by its improved range accuracy, resolution, range noise, higher measurement rates and the flexibility provided by its scanning capability. The previous rangefinders all operated with measurement rates < 50 Hz. OLA will operate at measurement rates of 100 Hz at ranges above 1 km and at 10 kHz at lower ranges. Many of these improvements over previous planetary lidars are made practical by the smaller operational ranges.

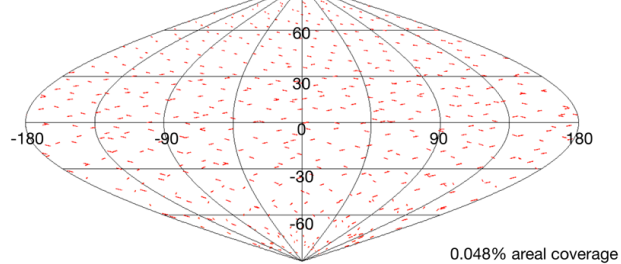
The high measurement rate and scanning capability have some advantages relative to typical point lidars, especially in the context of a small-body mission where spacecraft ground-track velocities are small. The inclusion of the high measurement rate and scanner in OLA make it possible to sample large portions of the asteroid surface without spending a substantial time in a long-period orbit to collect the required data (Fig. 1). This time-efficiency advantage is key to ensure the OSIRIS-REx mission can quickly obtain the global lidar-based surface measurements needed to validate prior image-based shape models, and to be able support hazard assessment for sampling. The scanning capability also has the design advantage of limiting any laser lifetime concerns for the instrument. Such laser lifetime issues tend to be the highest risk item for staring lidars that need to operate for a long time

**Fig. 1** View of coverage for staring lidar relative to OLA's scanning option for Bennu over same time period and operating with the same duty cycle

Using OLA Raster Scans



Using fixed nadir pointing LIDAR



(months to years) to collect sufficient data from many orbits. In the case of OLA, the scanning capability ensures the instrument achieves all of its scientific objectives within 100 hours of laser operations.

## 2 Operations

### 2.1 OLA Concept of Operations

The OLA concept of operations that constrained the instrument design is derived from the series of observation phases planned by the OSIRIS-REx mission team (Fig. 2). The mission phases are: Preliminary Survey, Orbital Phase A, Detailed Survey, Orbital Phase B, and Reconnaissance. Each of these phases has a different range from the asteroid and distinct spacecraft motions, pointing and local time coverage. See Lauretta et al. (2017) for a detailed description of the mission concept of operations. The operational mission phases for OLA have four distinct ranges and operational methods to characterize the asteroid. Local time is not a constraint for OLA operations. OLA makes use of a highly configurable scanner, and its ability to measure ranges from beyond 7 km and as close as  $\sim 10$  m at two measurement rates, to optimize characterization of the asteroid during these mission phases.

In the Preliminary Survey Phase, the asteroid location relative to the spacecraft is poorly known with respect to the observation geometry. OLA, therefore, is configured in a coarse pushbroom mode in which the scanner operates in a linear manner perpendicular to the spacecraft velocity vector. The scan angle is large enough to accommodate the navigational uncertainties and ensure the Bennu is in the field of view during some of the observation period. The measurement rate is 100 Hz, and the  $\sim 1.4$  m-diameter footprints are dispersed over the surface so as to ensure return signals are obtained given the initial spacecraft trajectory uncertainties, but with sufficient density to be able to identify the location of returns in supporting OCAMS imaging. As a result, OLA ranges support navigation and provide validation for an asteroid shape model obtained earlier in the mission using camera-based techniques.

**Table 2** A comparison of OLA to other planetary lidars. It should be noted that OLA is the only lidar with self-scanning capability. More details can be found in the following: MOLA (Smith et al. 2001); MLA (Cavanaugh et al. 2007); LOLA (Smith et al. 2010, 2017); NLR (Cole et al. 2000); Hayabusa (Mukai et al. 2002); Hayabusa 2 (Mizuno et al. 2017). The OLA resolution values include the bit resolution often quoted and the  $1\sigma$  range distributions for a stationary target

Instrument	Target	Range (km)	Accuracy (cm)	Resolution (cm)	Divergence ( $\mu$ rad)	Pulse energy (mJ)	Pulse rate (Hz)
MOLA	Mars	200–787	100	37.5	420	48	10
MLA	Mercury	< 1500	100	6	80	20	8
LOLA	Moon	< 150	10	$\sim 1$	100	2.5 (0.5 $\times$ 5)	28
NLR	Eros	0.1–300	32	32	100	15.3	1/8, 1, 2, 8
Hayabusa	Itokawa	$\leq 50$	< 1000	50	1700 $\times$ 700	10.5	1
Hayabusa 2	Ryugu	0.03–25	< 550	50	2400	15	1
OLA	Bennu	0.01–7	6 (L), 31 (H)	0.1 (bit), 1.1 (L), 2.6 (H)	100 (L), 200 (H)	0.01 (L), 0.7 (H)	10000 (L), 100 (H)

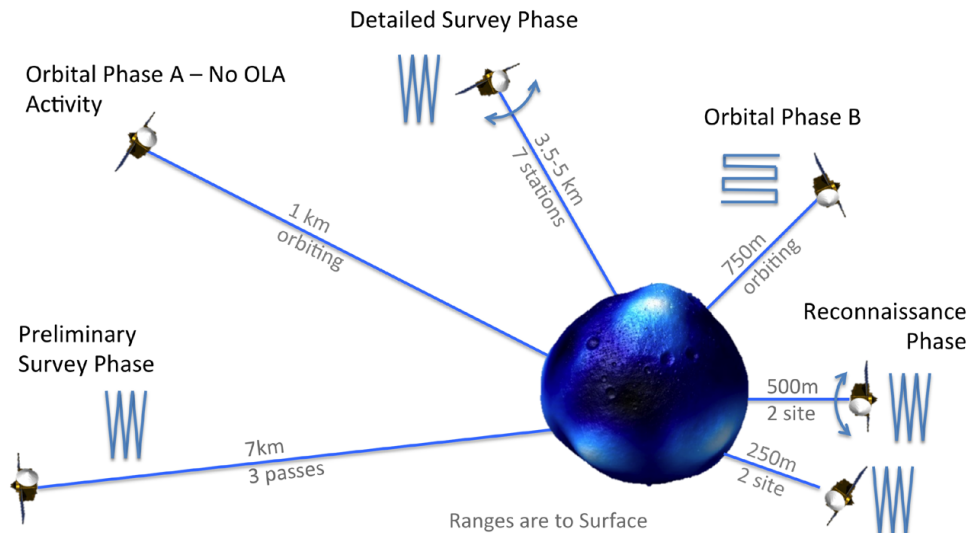


**Fig. 2** The OLA operation phases. OLA starts observing 7 km from the surface of the asteroid and was designed to extend to a 525 m reconnaissance of the sampling site. However, OLA is able to support reconnaissance observations near 200 m and lower. Some Orbital Phase A activity is being considered with emphasis on polar observations

As the spacecraft moves closer to the asteroid, the Detailed Survey Phase provides the opportunity for three near-stationary observations over the equator of the asteroid while the asteroid rotates in the measurement field over its 4.3 hr period. In this phase, the spacecraft slews in a North-South oscillation with a period of approximately 80 s. In order to maximize the coverage for OLA, an across-slew line-scan was selected. In contrast to the Preliminary Survey Phase, the scan is not sparse but will be configured for 100 Hz measurements every 200  $\mu$ rad of scanning motion. The width of  $\sim 20$  m for each slew is not a critical parameter because a three-slew areal coverage overlap is typical for OLA in this phase. The Baseball Diamond observations, consisting of two stations in the Northern hemisphere and another two in the Southern hemisphere, will allow coverage near the poles up to  $\pm 75^\circ$  latitude. Each OLA footprint will measure  $\sim 1$  m in diameter.

In Orbital Phase B, the spacecraft is  $\sim 750$  m from the surface of the asteroid. This is the main global data-collection phase for OLA, with the goal of enabling the production of a high-resolution global digital terrain model. In this phase, OLA is configured to operate in a manner similar to an imager. Using scan times of two to four minutes and a measurement rate of 10 kHz, OLA will take raster scans of the surface where the measurement spacing is equivalent to the beam divergence, thereby providing contiguous spots, each of  $\sim 7.5$  cm. A typical scan size will be about  $80 \text{ m} \times 80 \text{ m}$  on the surface of Bennu. These *images* are overlapping, thereby allowing a full shape model to be constructed through raster-to-raster registration.

In the Reconnaissance Phase, detailed topography is the required product for sample context and safe sampling. In this phase the spacecraft will slew across-track in support of imaging and spectroscopy. OLA will perform line-scans along the spacecraft ground-track direction to maximize OLA coverage. The coverage results in substantial overlap with a nominal three-times spot over-sampling thereby providing the potential to improve precision through spatial averaging. The OLA footprints in this phase measure  $\sim 3$  cm.

**Fig. 3** OLA consists of two subassemblies—The optical head unit (*right*) and the electronics unit (*left*)

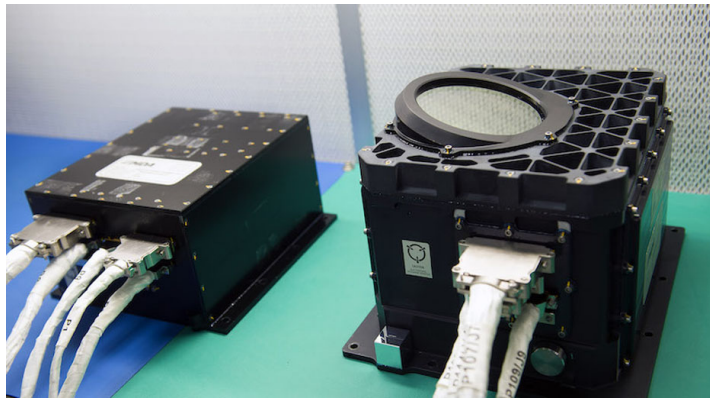


**Table 3** OLA as-built performance and key characteristics. Specifications are based on performance to a 3% Lambertian reflector

Specification	High energy	Low energy
Maximum operational range	9.0 km	1.2 km
Minimum operational range	0.26 km	0.036 km
Range accuracy ( $1\sigma$ )	< 0.31 m	< 0.06 m
Range precision ( $1\sigma$ )	< 0.026 m	< 0.011 m
Scanner field of regard	$\pm 6.7^\circ$ , $\pm 5.9^\circ$	$\pm 6.7^\circ$ , $\pm 5.9^\circ$
Scanner precision	< 20 $\mu$ rad	< 20 $\mu$ rad
Laser divergence (1/e)	200 $\mu$ rad	100 $\mu$ rad
False alarms	< $10^{-6}$	< $10^{-6}$
Probability of detection	> 99.99%	> 99.99%
Clear aperture	75 mm	75 mm
Pulse energy	0.7 mJ	10 $\mu$ J
Pulse duration	5 ns	1 ns
Mass—electronics		7.6 kg
Mass—optical head		13.8 kg
Power—nominal		59 W
Power—standby		43 W
Dimensions—electronics (mm)	265 L $\times$ 250 W $\times$ 142 H	
Dimensions—optical head (mm)	270 L $\times$ 320 W $\times$ 230 H	

### 3 OLA Instrument Design

#### 3.1 Design and Performance Overview

OLA consists of two subassemblies (Fig. 3): a sensorhead (which contains all of the optics, lasers, and circuitry to both drive the lasers and detect return signals) and the main electronics (which contains all of the system avionics such as signal processing, power, spacecraft communication, and time-of-flight circuitry). The OLA as-built performance is outlined in Table 3. Comparison with Table 1 shows that OLA exceeds its specifications in all but *Scanner Field of Regard*. During the design phase, a compromise was made to increase the mechanical robustness of the scanning system and the scanning range was reduced in one axis from  $\pm 10^\circ$  to  $\pm 6^\circ$ . This change does not compromise the utility of OLA in the mission because the current concept of operations requires no more than  $\pm 3^\circ$  in this axis.



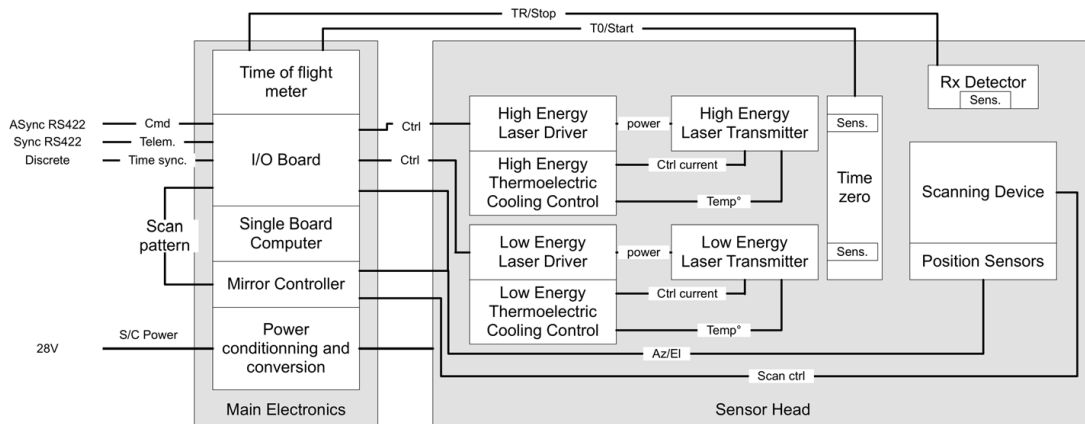


**Fig. 4** OLA block diagram

## 3.2 Hardware Description

The electronics for OLA (functionally depicted in Fig. 4) are divided between the two OLA assemblies.

### 3.2.1 Main Electronics Unit

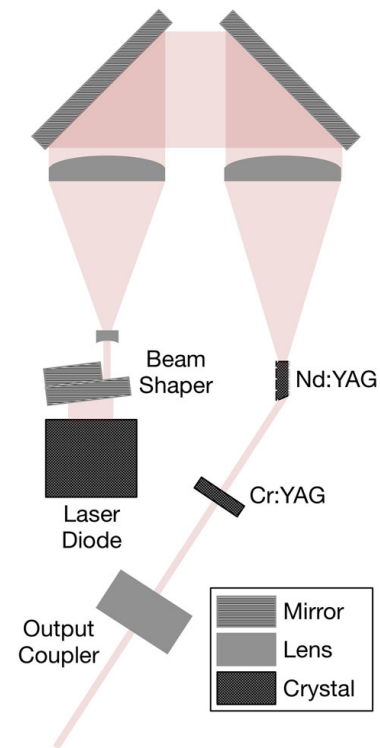
The Main Electronics Unit is built in a backplane configuration with the backplane providing the interconnections between circuit card assemblies. It contains the main power circuit card assembly (CCA) that provides electromagnetic compatibility filtering and power conditioning of the spacecraft bus power using DC-to-DC converters. A second auxiliary power CCA provides additional voltage rails for the various CCAs in the OLA assembly. An Input/Output CCA provides connectivity with the spacecraft. This connectivity consists of an asynchronous RS-422 channel and discrete lines for managing safety interlocks. An Aitech S950 single-board computer (SBC) provides the command and control functionality for OLA.

A Time-Interval Meter (TIM) CCA provides the absolute timing differences between the outgoing pulse as measured by a silicon pin diode and the received pulse as measured by the receiver silicon avalanche photodiode (APD). The timing accuracy has been shown to be better than 40 ps based on ranging measurement precisions of 1.1 cm  $1\sigma$ . The timing signals are distributed to the TIM by low voltage differential signals (LVDS). This CCA also measures the peak amplitude of the outgoing and received pulses. This information is used for science reasons, health trending and for a minor range correction. A mirror controller provides the commands and closed-loop control to OLA's dexterous 2D scanning mirror. This mirror can operate in three modes: staring, linear, and raster.

### 3.2.2 Sensor Head

The OLA Optical Assembly contains the receiver and transmitter optics, the scanning mirror, the lasers and the electronics that benefit from close proximity to these components. The OLA receiver is based on a silicon APD with a 800  $\mu\text{m}$  diameter active area biased at  $\sim 300$  V. The Receiver uses a constant-fraction discriminator (CFD) to minimize range-walk effects (e.g., Popescu 2012). The CFD threshold has two selectable ranges: a nominal range and a lower threshold that can be used for a minor extension of the maximum range of the instrument with an increase in false returns.

**Fig. 5** The OLA high-energy laser transmitter is a diode-pumped solid state Nd:YAG laser with a design based on the Phoenix Mars lidar instrument



OLA contains two independent laser transmitters. The low-energy laser transmitter (LELT) and the high-energy laser transmitter (HELT) each have independent time-zero (T0) detectors that provide the outgoing pulse reference time. One CCA is used for the LELT and one for the HELT. As the signal levels are significant from the outgoing laser beam samplers, silicon pin diodes are used instead of APDs. These assemblies provide a digital timing signal and an analogue peak amplitude signal for each channel back to the time-interval meter (TIM) CCA in the main electronics unit.

The LELT operates at 10  $\mu\text{J}$ –1 ns pulse length and a 10 kHz pulse repetition rate. It operates at ranges from 1 km to near the surface of the asteroid. It is a small diode-pumped microchip laser with a passive Cr:YAG Q-switch integrated into the lasing medium through diffusion. It is cooled by two thermoelectric coolers. It is collimated using a Keplerian beam expander to a beam diameter of 15 mm ( $1/e^2$ ) and a beam divergence of 100  $\mu\text{rad}$  ( $1/e$ ). A beam pick-off is used along with a pin diode-based receiver to provide the T0 signal to the timing circuit. This signal also provides laser health data.

The OLA HELT, shown in Fig. 5, is a more conventional diode-pumped Nd:YAG solid state laser that also operates at 1064 nm and at 0.7 mJ. It traces its heritage directly to the Phoenix Mars MET lidar (Whiteway et al. 2008). It consists of an electrically pumped laser diode array at 808 nm that undergoes beam shaping by both reflective and refractive optics. The Nd:YAG crystal provides one facet of the laser cavity and is longitudinally end-pumped. The diode array and the Nd:YAG crystal are individually cooled to precise setpoint temperatures to maximize laser efficiency. The opposite end of the YAG crystal is Brewster cut and provides a linearly polarized output. A passive Cr:YAG Q-switch saturable absorber is used to create the laser pulse. An output coupler of 80% reflectance completes the laser cavity. It is collimated using a Keplerian beam expander to a beam diameter of 10 mm ( $1/e^2$ ) and a beam divergence of 200  $\mu\text{rad}$  ( $1/e$ ). A beam pick-off is used along with a pin diode-based receiver to provide a T0 signal to the timing circuit as well as to terminate the electrical pump pulse.

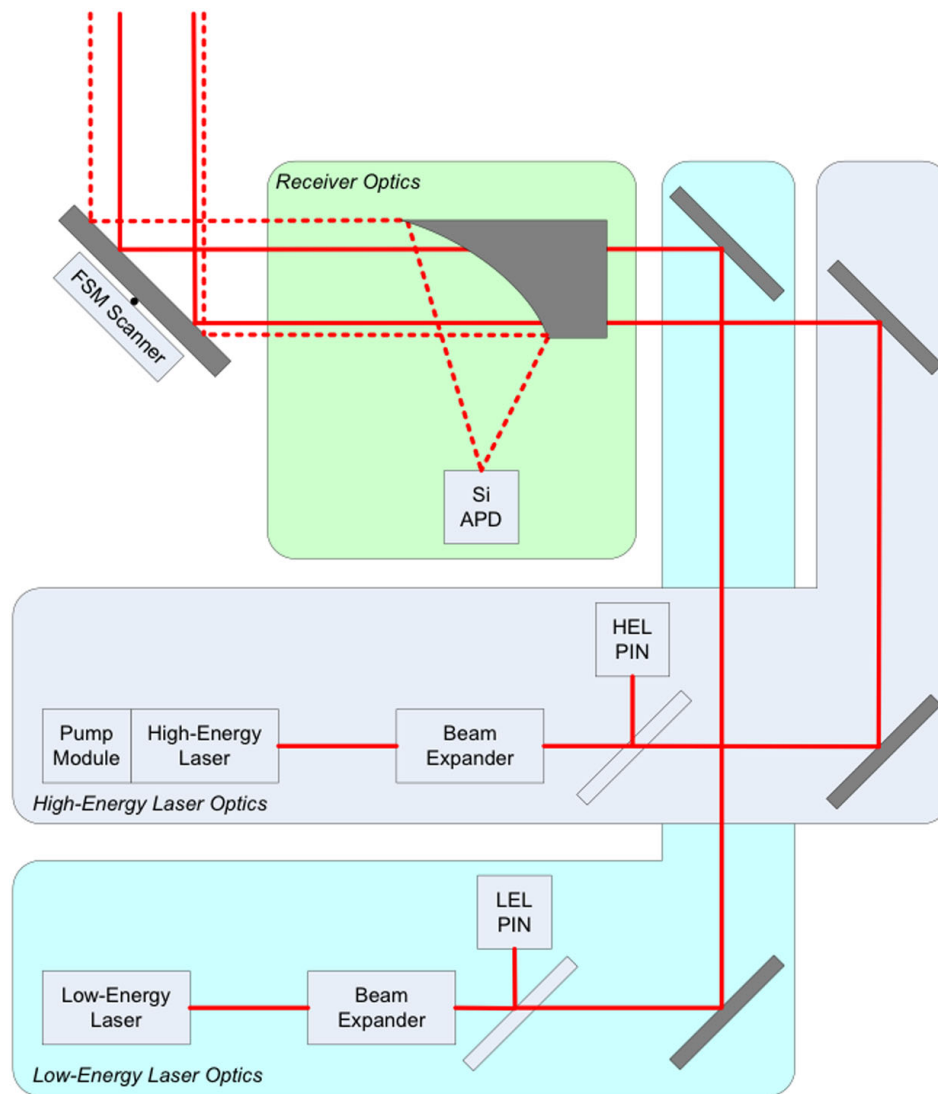


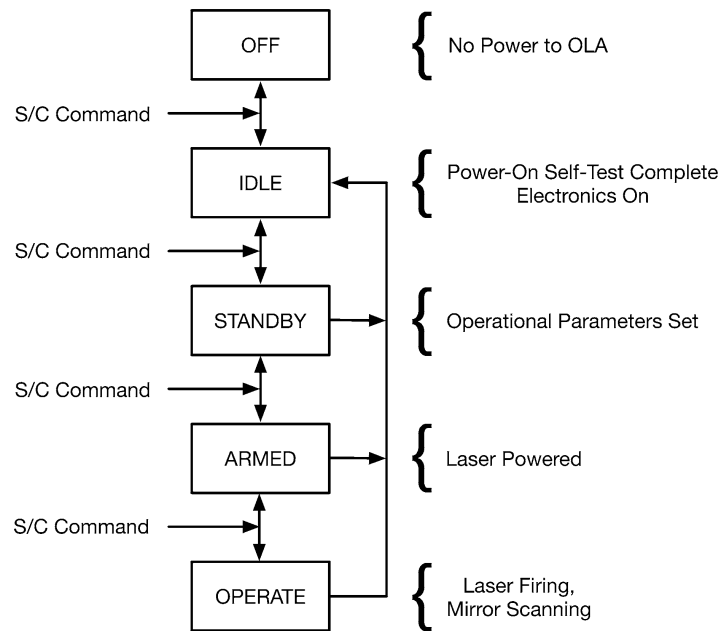
**Fig. 6** A schematic diagram of the OLA optical configuration

Two cooler controllers are used to control the temperature of the laser diodes and the Nd:YAG crystals. The LELT requires a single thermoelectric cooler as the diode and the crystals are in close proximity and well temperature matched. The HELT requires two separate coolers due to the physical separation of the elements. The two coolers are set to a temperature difference that maximizes the efficiency of the laser. The nominal set points are all within a 10 degree span about room temperature.

The optical layout for OLA is shown in Fig. 6. The layout is extremely simple with the only elements with optical power being a beam expander in each of the transmitter optical paths. These beam expanders are used to tailor the beam divergences to 200  $\mu\text{rad}$  for the HELT and 100  $\mu\text{rad}$  for the LELT. Low reflectivity beam pickoffs are used to capture the T0 signals.

The receiver is a 76 mm diameter off-axis parabolic (OAP) mirror with a parent focal length of 76.2 mm and a slant focal length of 152.4 mm operating in a 90° configuration. Two apertures in the OAP are used to allow the outgoing transmitter beams to be coaxially aligned with the receiver FOV. The two-axis flexure-based scanning mirror provides simultaneous steering of the receiver FOV and the outgoing laser beams.

**Fig. 7** OLA state diagram and general command flow



### 3.2.3 Mechanical Spacecraft Interface and Thermal Design

Each of the two OLA subassemblies is wet-mounted to the deck of the spacecraft (i.e., OLA is bonded to the surface of the OSIRIS-REx science deck using thermal adhesive) to maximize heat transfer away from OLA during operation of the system. The walls of the sensor head are sufficiently thick to: (1) provide structural support; (2) provide radiation shielding from the space environment; and, (3) provide efficient heat transfer throughout the chassis and (very nearly) homogenous structural temperatures during operation. Such homogenous temperatures reduce the effects of thermal distortions on the optical path, thus providing a stable platform for making observations and minimizing any movement of the laser beams and/or receiver.

## 3.3 Software

OLA command and data handling functions are handled by a general purpose single-board computer. The Aitech S950 single-board computer runs at 400 MHz to reduce power consumption relative to the highest clock-speed model. It is running Wind River VxWorks 5.5 as an operating system. The software uses object-oriented design in C++.

### 3.3.1 Architecture

The software architecture of OLA allows a number of predefined instrument states and carefully controls the transitions between them. The states and allowed state transitions are shown in Fig. 7. OLA can exist in the following powered states: Initialize, Idle, Standby, Armed, Operate, Diagnostic and Failed.

Upon powering up, OLA conducts a Power-On Self-Test (POST), which verifies that internal power rails are within range, calibration voltages are nominal and the memory checksum is correct. A successful POST puts OLA into the IDLE state. Failure of POST (nominally) results in a category 1 (CAT1) error that logs the error and transitions to IDLE.

After POST completes, OLA transitions to the IDLE state and expects a spacecraft clock (SCLK) time-update message every second along with a time sync discrete signal. These

are used to precisely synchronize the OLA internal clock to Spacecraft time. From this point forward, SCLK updates are reported in telemetry along with the internal OLA clock time. Should no spacecraft time update message be received, the OLA clock reports its internal time since power-up.

In the IDLE state, OLA can receive an updated Configure OLA file (or an update error category (CAT) Response Table file) and OLA then ensures that the parameters are within specified limits. A failure of this check causes a CAT1 error that logs the error and causes a transition to IDLE.

Upon receiving a command to enter the Standby State, OLA begins heating of critical electrical components to ensure that they are within their operational temperature limits. This nominally takes 5 minutes. This warm-up time is managed operationally through script parameters.

Once OLA is commanded into the Operate State, via a Scan command with warm-up and scan duration time-out parameters specified, the following steps occur:

**Laser—Warm-up, no data** To ensure that the OLA laser is operating at peak performance, the entire system is first commanded to operate without data being sent. This is to achieve thermal equilibrium between the thermoelectric coolers and the surrounding structure). Warm-up time should nominally be 1000 s.

**Scan (Operate)** Following completion of the warm-up period, OLA proceeds to scan the mirror and to report scan data as telemetry, provided the scan time-out parameter specified is greater than zero.

**Scan Timeout** A scan duration timeout is sent as a parameter within the Scan command, and sets a time out duration to transition back to the Standby State in the event that:

- The required continuous scan operation time has expired (for example, a commanded linear scan for X minutes).
- The commanded time for a single scan has been exceeded (for example, a single raster scan of known duration).

**S/C Monitoring** The spacecraft does not parse or act upon OLA science data, with the following two exceptions:

**S/C Check One** Once OLA is commanded in the Operate State, the OSIRIS-REx spacecraft checks for the reception of an OLA High Priority data packet. If this check fails, the spacecraft attempts to reinitiate OLA operation (as determined by the command sequence or block).

**S/C Check Two** The reception of a SAFE\_ME request from OLA to the spacecraft causes OLA to be declared SAFE, and power is removed from the instrument.

The spacecraft can access in real time some OLA data that is contained in the science data header. In particular, there is an average range field (based on the 500 measurements for which the header applies) that can be used by the spacecraft for camera focusing or for other purposes where 20 Hz measurements of range to the surface are needed.

### 3.3.2 OLA Scan Configuration

The main OLA command is a *Start Scan* command. The key parameters for a scan are shown in Table 4. OLA scans can be made with either the HELT or the LELT. Once the laser transmitter is chosen, the measurement rate is set by the fundamental laser repetition rate. A scan duration provides the length of the scan either by pattern repetition in a *Continuous* scan or

**Table 4** The key fields in the OLA Start Scan command

Field	Description	Value
Laser select	Specify laser	HELT or LELET
Scan repetition	Enables a single pass through a pattern or repetitive passes	single or continuous
Spot angular spacing	Angular separation between adjacent spots	0.05–10 mrad
Scan pattern	Define measurement pattern	Raster, linear or fixed
Scan orientation	Direction of fast mirror travel	Azimuth or elevation
Window size	Window size (azimuth or elevation)	0–340 mrad
Window center	Center of scan (azimuth or elevation)	0–340 mrad
Scan duration	Duration of scan	0–65535 s
Receiver setting	Choose receiver threshold	Nominal or low
Decimation	Choose decimation	None, 2×, 10×, 100×, 1000×

by providing a maximum time-out value in a *Single* scan. A lower receiver threshold than the nominal can be set to improve OLA's range performance at the expense of an increased false-alarm rate. The majority of the remaining configuration relates to the scanning mirror parameters.

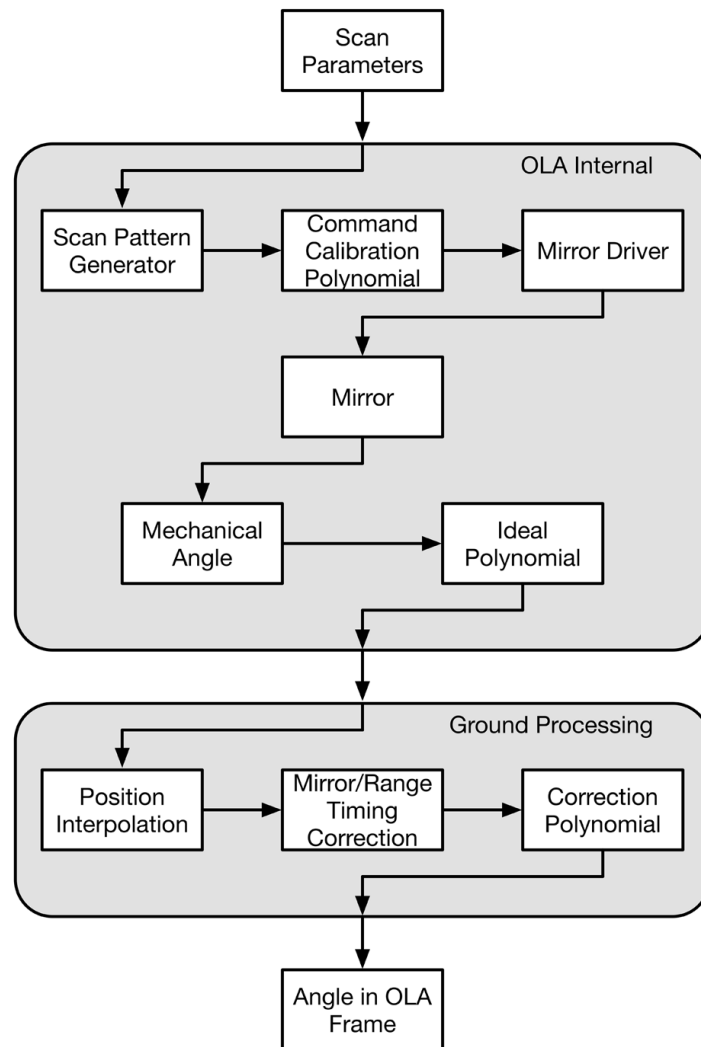
The OLA scanner can be configured in three scan patterns. A *Fixed* or staring pattern is not currently planned for flight, but was implemented to support test configurations. The two operational patterns are a *Linear* or line-scan pattern and a *Raster* or area-scan pattern. Each of the two operational patterns can be configured with their prime axis in the azimuthal or elevation direction. The center of the pattern can be specified within the allowed scan window to allow arbitrary instrument-level pointing. The scanner speed is set by specifying the angular spacing between spots. This will normally be set at 0.1 mrad for contiguous spots for the LELET. The scan pattern generator interprets this value as the highest mirror velocity. The highest mirror velocity occurs at the center of the scan and the extent of this region varies with the scan pattern as it is limited by the span required to accelerate and decelerate the mirror.

OLA provides the ability to parse and prioritize its data in order to allow management of OLA data volumes, which can be large given OLA's 10 kHz measurement rate. If Data Decimation is required, control is achieved through the Scan command with the decimation parameter specified (nominally, 2, 10, 100, or 1000). Scan Data will then be arranged into Decimated Data (tagged as High Priority Science Data) and Undecimated Data (tagged as Low Priority Science Data). For example, applying a 10-fold data decimation scheme would result in 1 scan point in every 10 being put into a High Priority data packet, while all 10 scan points would be put into a Low Priority data packet. The spacecraft has the option to not transmit the Low Priority packet.

### 3.3.3 Measurement Data

The key contents of an OLA measurement point consist of a range (mm resolution), a time (1  $\mu$ s resolution), mirror angles (0.025 mrad resolution), and incoming and outgoing intensities (14-bit values). A reduced data record is shown in Table 5. These values undergo a series of calibrations in the ground processing software (Figs. 8 and 9). As shown in Fig. 8, OLA has a set of ideal mirror parameters that are polynomials relating commanded mirror driver voltages to desired coordinates in azimuth and elevation. A similar set of polynomials

**Fig. 8** The OLA mirror command and pointing correction approach



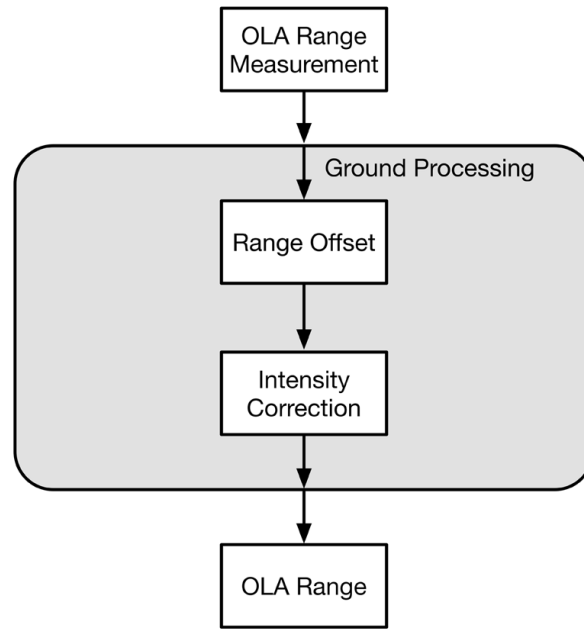
provide angular mirror positions from mirror position voltage readings. A series of ground-based corrections are required to further calibrate these positions. The first of these requires a position interpolation and timing correction to account for electronic timing differences between mirror positions and the laser pulse timing. For OLA, this timing difference is  $\sim 130 \mu\text{s}$  or approximately 1.3 measurement times when using the LELET and  $\sim 9650 \mu\text{s}$  for the HELT. These reported positions are further corrected through 15 coefficient correction polynomials that are functions of the reported azimuthal and elevation coordinates.

Range data corrections (Fig. 9) require a range offset that is  $\sim 0.75 \text{ m}$  and a range-intensity correction. The range-intensity correction is minor ( $\sim 2 \text{ cm}$ ) over most of the dynamic range of OLA, as would be expected for a well-designed CFD-based receiver. For the lowest 3% of the dynamic range, the correction increases to as much as 8 cm for the lowest amplitude detection. Additional detail is provided in Sect. 4.3.

## 4 Instrument Calibration and Characterization

### 4.1 OLA Test and Calibration Facilities

OLA test and calibrations took place at three major facilities. The range calibrations, mirror calibrations, and the vibration tests were conducted at MDA's Brampton, Ontario, Canada,

**Fig. 9** OLA range correction**Table 5** The key fields in the OLA data record

Field	Description	Value
Scan ID	Unique scan identifier passed back from command	unique integer
Time sync fields	Fields required to reference a scan to spacecraft times	various
Range	Integer range in mm	0 to 16777215 mm
Azimuth	Measured mirror azimuth	-170 to +170 mrad (0.025 mrad)
Elevation	Measured mirror elevation	-170 to +170 mrad (0.025 mrad)
Intensity t0	Outgoing pulse amplitude	0 to 16383 (arb. units)
Intensity tr	Incoming pulse amplitude	0 to 16383 (arb. units)
Flag	Assessment of valid return	Valid, valid (overflow), null

facility. The OLA-specific facility includes a calibration wall at a range of 27 m (Fig. 10). This wall has a series of surveyed targets to allow the computation of the mirror correction polynomials. These targets are surveyed relative to a test stand that provides a known and repeatable position for OLA test and calibrations. Survey errors of each target relative to the test stand have been determined by the survey team to be normally distributed with a  $3\sigma$  magnitude of 0.085 mrad. The test stand is shown in Fig. 11. Note the red assembly over the OLA aperture. This test fixture consists of a series of neutral density filters that allow OLA to operate to a high reflectivity target at ranges down to 8 m.

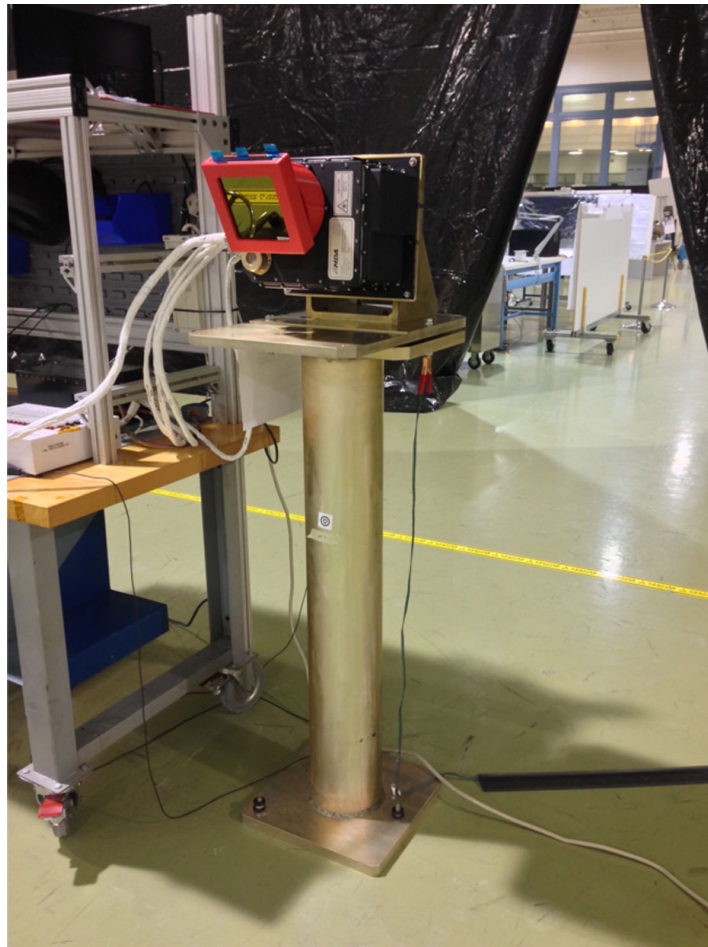
The thermal vacuum tests were conducted at the facilities housed at the Centre for Research in Earth and Space Science (CRESS) at York University in Toronto, Ontario, Canada. This chamber had an anti-reflection-coated window installed at the end of the chamber that allowed OLA to view a reduced field set of targets similar to that on the 27 m calibration wall but at 8 m. These targets were used to assess OLA's relative pointing performance over temperature.



**Fig. 10** The OLA calibration wall is shown. An individual target is shown in the *inset*



**Fig. 11** A view of OLA on its calibration stand



A further unique test facility was a long-distance range situated near York University. This outdoor range was accessed using a specifically constructed clean box that allowed OLA to be safely operated while viewing targets consisting of the York University physical plant smokestack at approximately 900 m and a student residence at approximately 1.2 km.

**Fig. 12** The thermal vacuum (TVAC) facilities at York University. OLA can be seen just behind the window

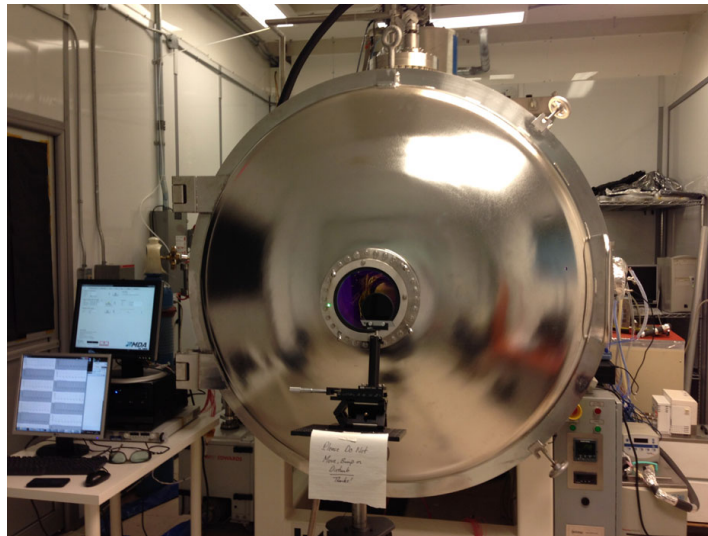


**Fig. 13** The view from the long-range test facility



The view from this test range is shown in Fig. 13. This facility was used to validate the long-range OLA performance model and to demonstrate the co-alignment of the transmitters with the OLA receiver.

## 4.2 Ambient Angular Mirror Calibration

The angular calibration for both the LEIT and HELT subsystems of OLA provides a correction of reported mirror position to the actual mirror position, thereby allowing the measured spots to be properly located in angular space. These corrections are discussed in Sect. 3.3.3. Calibrations were obtained from scan data collected at MDA's Brampton facility on both the short-range (8 m) and the longer-range (27 m) surveyed target walls. These walls have targets that are easily identified in the intensity measurement of OLA. To operate at these ranges, a set of neutral density filters was used that attenuated both the outgoing laser energy and the incoming signal.

Dynamic rastered scan data was collected by both the HELT and the LEIT (e.g., Fig. 14) for a number of surveyed targets in the short-range and long-range areas. The surveyed targets in each room were scanned twice in the azimuthal direction and twice in the elevation direction (direction referenced to that of the fastest mirror motion) for both the HELT and LEIT, for a total of eight scans of each target per room. The target centroids for each scan were calculated and compared to the surveyed positions.

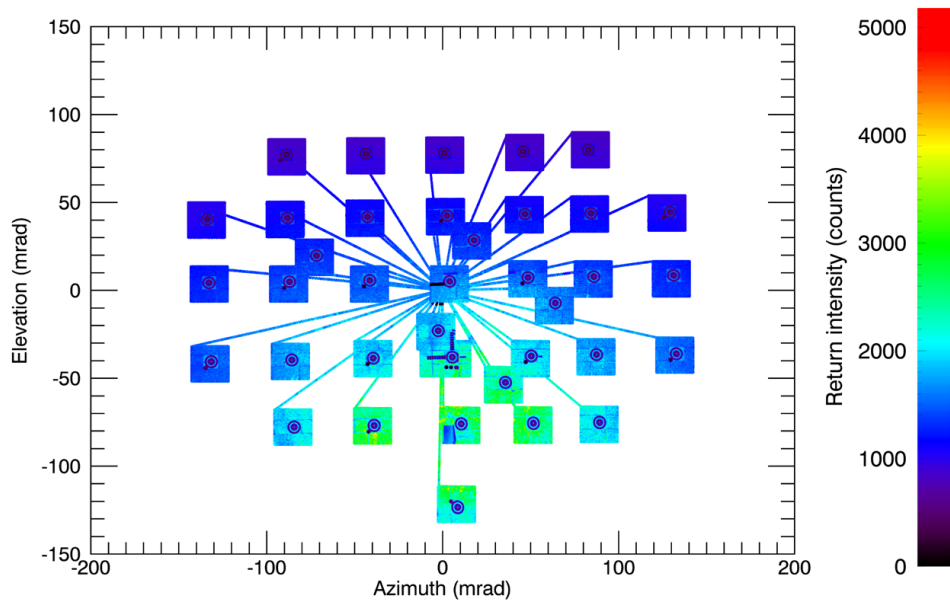


**Fig. 14** LELT dynamic scans of the Task Area target wall

**Table 6** The measured deviations between the measured and actual target centroids taken during the OLA ambient angular mirror calibration

LELT	Azimuth ( $\mu$ rad)	Elevation ( $\mu$ rad)
Minimum	-119	-172
Maximum	128	150
Standard deviation	41	47
HELT	Azimuth ( $\mu$ rad)	Elevation ( $\mu$ rad)
Minimum	-110	-71
Maximum	105	69
Standard deviation	44	27

Angular calibration was achieved by fitting a two-dimensional (2D) Taylor Polynomial (of 4th order) to the complete set of dynamic scan angular data. The result of this calibration is a 2D polynomial correction that will be applied to the collected azimuth and elevation data during ground data processing. A similar approach provided a command polynomial that is integrated into the instrument to allow mirror behaviors consistent with the command dictionary. After applying the correction polynomials, the instrument achieves pointing across the field of better than 50  $\mu$ rad standard deviation for both the Az and El axes. Detailed values are found in Table 6.

### 4.3 Ambient Range Calibration

Both LELT and HELT range calibrations were performed at the MDA facilities. Range calibrations were done in a staring mode to a surveyed target. OLA was mounted to a surveyed stand as shown in Fig. 11. The range measurement precision of a single measurement is well characterized by a normal distribution of standard deviation of 1.1 cm for the LELET and 2.6 cm for the HELT. The calibration consisted of determining the range offset between the reported range and the actual range. Although this value could have been integrated

into the instrument, the decision was made to incorporate this value into the ground-based calibration pipeline. The range offsets are  $-869$  mm for the LELT and  $-1269$  mm for the HELT.

An additional range-intensity correction was determined using a variable neutral density filter to correct for a small range dependence ( $\sim 8$  cm) on the magnitude of the received signal. This correction is small and well behaved for the upper 97% of the dynamic range of the instruments ( $\sim 2$  cm for both the HELT and the LELT). For the lower 3% of the dynamic range, this correction can approach 12 to 15 cm for the smallest detectable signals. This behavior is well-known for constant-fraction discriminators. This correction is implemented in the ground data processing system.

#### 4.4 Additional Range Calibration Considerations

During testing of OLA, it was noted that the LELT exhibits a dual-mode behavior, in which the T0 signals vary shot to shot. This effect was observed on other laser units and appears fundamental to the design of these microchip lasers and is probably due to two spatial modes being excited in the laser. Each of these modes has a small amplitude and pulse duration difference and therefore requires minor differences in calibration. These two modes are interleaved and combined produce the 10 kHz measurement rate of OLA. In testing, the laser operates stably with this interleaved behavior for many minutes and only rarely sequentially repeats a mode. The data from the range-intensity correction was separated into the two modes and analyzed separately. The consequences of not applying these curves is typically 2–3 mm but can be higher in the lowest 3% of the instrument's dynamic range. Each mode will have its own range-intensity curve applied in the OLA calibration pipeline.

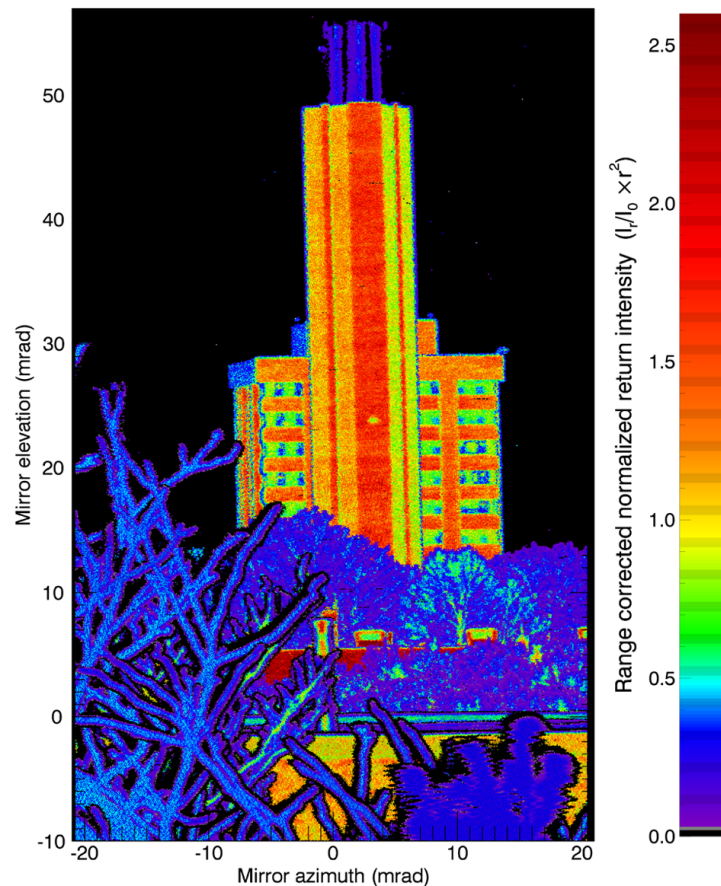
#### 4.5 Long-Range Test

Range tests to validate the long-range performance of OLA and to validate the long-range alignment were conducted at facilities near York University in April 2015. They also provide an excellent example of OLA's scanning capabilities. A top floor (mezzanine) window allowed access to targets of opportunity in the immediate neighborhood. Figure 13 shows the targets used for these tests (inside red circle): The York University concrete smoke stack (referenced as YU Smoke Stack target), at the center of the picture, is roughly 890 m in range from the approximate position of OLA. A student residence, constructed largely of concrete, is  $\sim 300$  m behind the smoke stack, (referenced as Building behind YU Smoke Stack target), or roughly 1200 m in range from OLA. Foreground foliage and a portion of the top of a building immediately across the street were also scanned during these tests. 3D point clouds of the target with both the LELT and HELT were acquired dynamically by raster scanning the mirror (Fig. 15 and Fig. 16, respectively). These scans are illustrative of the relative range and resolution performance of the two transmitters.

Data points representative of each target, for both the LELT and HELT, were selected and used together with an analytical range performance model to demonstrate the flight-range capability of OLA. The performance matched the prediction within experimental error.

At a height of 22 m a pair of aircraft warning lights and a security camera are mounted on the front surface of the YU smoke stack (Fig. 17). This feature is apparent in the LELT point cloud (Fig. 15) as an area of reduced return intensity. Isolating this area of the point cloud, a feature with a depth of approximately 20 cm (Fig. 18) can be seen protruding from the surface of the YU Smoke Stack. A gridded surface of this same area (Fig. 19), color coded to represent deviation from the front surface of the YU Smoke Stack, clearly shows

**Fig. 15** A LEIT raster scan in the mirror frame of reference. The *color scale* represents the range-corrected normalized return intensity



the security camera protrusion to the right, and the metal surface inset into the concrete structure. The presence of the aircraft warning lights is apparent in the colored surface, but the recorded ranges do not accurately represent the depth that the lights protrude from the YU Smoke Stack. This is due to the fact that at a range of 800 m, the laser spot size is approximately 8 cm—larger than the width of the warning lights. Thus OLA recorded ranges that are a convolution of return signal from the warning lights, and from the metal plate behind the lights. Nonetheless, it provides an excellent demonstration of the imaging performance of OLA.

#### 4.6 OLA Step Characterization

In order to validate the understanding of the receiver behavior in the presence of steps, an additional characterization test was performed. These situations can arise when a portion of the lidar beam interacts with the top of a block while the remaining portion interacts with the base topography. To simulate this situation, a test target was fabricated that allows a variable portion of the lidar beam to interact with the top of the target while also allowing a configurable step height (Fig. 20).

An example dataset is shown in Fig. 21. This dataset shows that for steps less than 0.5 m, OLA provides a weighted average range (black curve). For steps greater than 0.5 m, OLA provides a result that is consistent with the nearest target or farthest target, depending on the relative portion of the signal on each. We found the results consistent with a 100 MHz receiver bandwidth. Given the divergence of each of the OLA transmitters, it is expected that consideration of this behavior will not be required during any but Preliminary Survey and Detailed Survey.

**Fig. 16** A HELT raster scan in the mirror frame of reference. The *color scale* represents the range corrected normalized return intensity

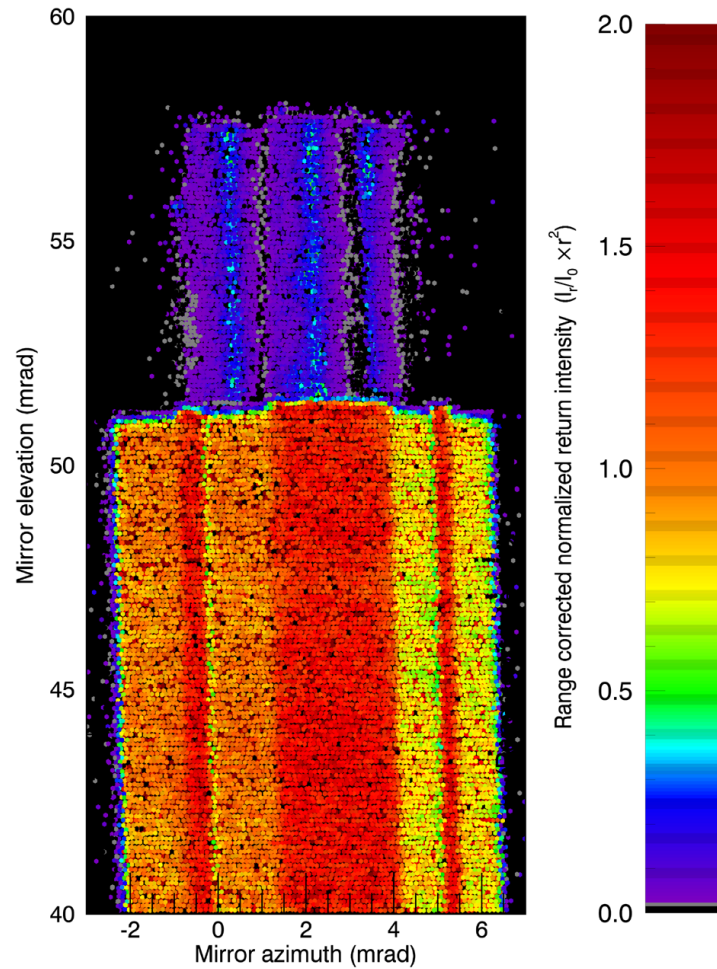


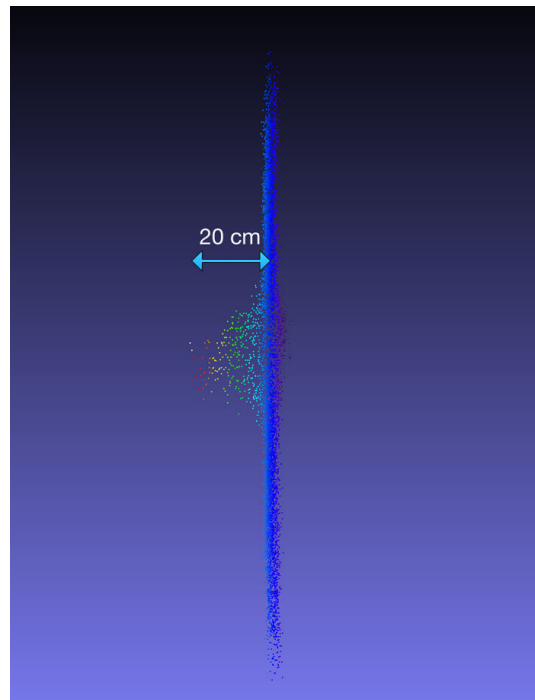
**Fig. 17** A photograph of the aircraft warning lights and security camera as mounted on the side of the York University Stack



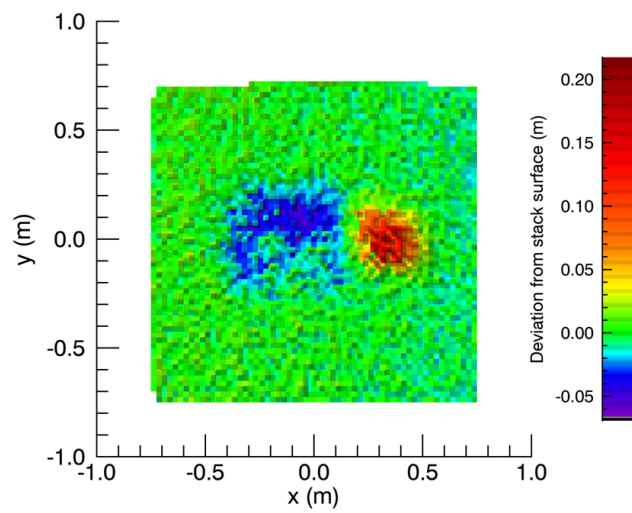
## 4.7 Environmental Testing

OLA was subjected to a standard set of environmental tests that included thermal vacuum testing, random vibration testing and electromagnetic compatibility (EMC) testing. These tests were tailored to the requirements of the OSIRIS-REx mission. The tests went without

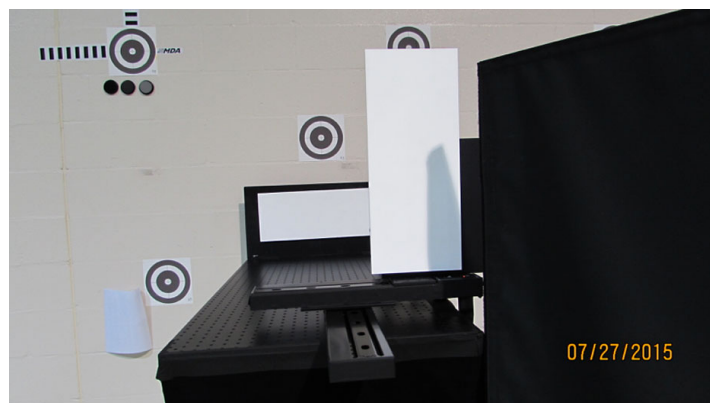
**Fig. 18** An OLA point cloud of York University Stack security camera is shown edge on



**Fig. 19** A Gridded surface showing the aircraft warning lights and security camera scanned by the LEELT at a range of 900 m



**Fig. 20** A photograph of the OLA step characterization experimental apparatus



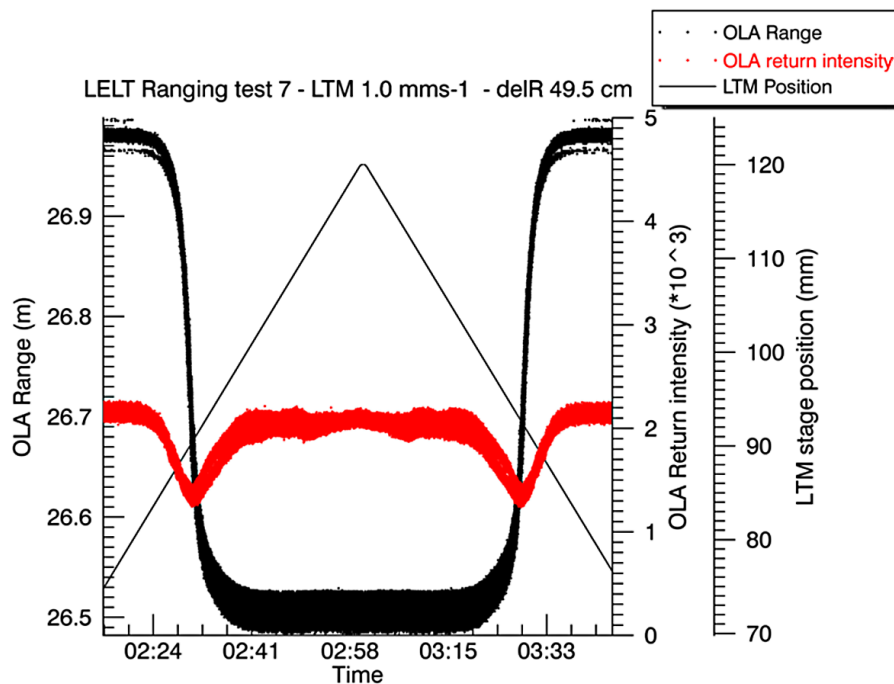


**Fig. 21** The OLA step characterization Results. The results (*thick black line*) demonstrate that for small steps, the reported range transitions gracefully between the top and base measurements. The reported range is approximately a photon-weighted average of the ranges of the objects sampled by the incident beam

notable problems with the exception of the vibration test of the optical head unit, where a resonant coupling between a chassis mode and the scanning mirror was discovered through a failure of the scanning mirror mechanism. This problem was rectified by strengthening the chassis through the redesign of the optical head unit cover that separates these resonances, and this design change resulted in a successful vibration test. This design change can be seen in Fig. 3 where the waffled cover is apparent.

OLA thermal vacuum testing consisted of typically shaped thermal cycles with extrema set by mission thermal modelling combined with a single cycle with 5 °C baseplate temperature steps from −5 °C to 30 °C. These temperature steps were used to validate the OLA specifications over temperature. OLA was mounted near a window at one end of the chamber (Fig. 12) in view of a target wall at an 8 m distance with a series of targets of the same size and shape as those used on the calibration walls at the MDA facilities.

These targets were used along with an external reference to assess the pointing changes of OLA over temperature. There was no significant trend in the elevation axis for the HELT or the LELT with the measurements following a linear trend and bounded by an  $\sim 100 \mu\text{rad}$  change over the 35 °C operational range. In the elevation axis, the performance for the LELT was bounded by a  $\sim 250 \mu\text{rad}$  change and the HELT by a larger  $\sim 600 \mu\text{rad}$  change. All of these changes are roughly linear and well behaved. It should be noted that all OLA observations and their subsequent data processing do not assume long-term absolute pointing stability but only short-term relative pointing stability.

A more important assessment of pointing for OSIRIS-REx is an evaluation of relative pointing. This can be thought of as a field distortion in camera terms and is important because the majority of the OLA data analysis is dependent on these datasets collected over minutes and are less dependent on absolute pointing knowledge. Relative pointing was bounded during the TVAC tests to be less than  $\sim 120 \mu\text{rad}$  in the diagonal over the temper-



ature range. This amounts to 1.2 spot diameters over a typical raster scan field of 1400 spot diameters.

Range measurements changes were also shown to be slowly varying and bounded by 4.9 cm for the LETL and 295 mm for the HELT. Since the OLA data processing algorithms do not rely on long-term stability but only stability over short spans (i.e., individual slews in Detailed Survey or single Orbital Phase B scans), it is expected that in-flight topographical performance will approach that of the inherent instrument noise of 1.1 cm and 2.6 cm.

## 5 Summary

OLA is a new class of planetary exploration lidar that provides measurement rates 100 to 10,000 times those of previous lidars and provides a flexible scanning system that allows a slow moving spacecraft to make use of these measurement rates. The increased measurement rate and scanner allows OLA to measure the shape of the entire asteroid without spending an extremely long time in orbit. This time advantage is key to ensure the OSIRIS-REx mission can quickly obtain the surface topography measurements needed to verify prior image-based shape models, and to be able support hazard assessment for the critical sampling activity. OLA is expected to map the surface of Bennu with 7 cm precision globally, thereby providing unprecedented topography of an asteroid. OLA also provides precise ranges for spacecraft navigation, thereby adding confidence and improving the efficiency of navigating a spacecraft around this small body.

**Acknowledgements** There are many important contributors who could not be included in the author list. These contributors include staff at MDA, Teledyne Optech, CSA, York University, University of British Columbia, University of Arizona, Johns Hopkins University Applied Physics Laboratory, Lockheed Martin and NASA Goddard Spaceflight Center. The instrument build and Canadian science support was provided by a contract with the Canadian Space Agency. The United States team contribution was supported by the National Aeronautics and Space Administration under Contract NNM10AA11C and NNG12FD66C issued through the New Frontiers Program.

## References

- O.S. Barnouin-Jha, A.F. Cheng, T. Mukai, S. Abe, N. Hirata, R. Nakamura, R.W. Gaskell, J. Saito, B.E. Clark, Small-scale topography of 25143 Itokawa from the Hayabusa laser altimeter. *Icarus* **198**(1), 108–124 (2008)
- R. Binzel, Regolith x-ray imaging spectrometer (REXIS) aboard the OSIRIS-REx asteroid sample return mission. *Space Sci. Rev.* (2017, this issue)
- J.F. Cavanaugh, J.C. Smith, X. Sun, A.E. Bartels, L. Ramos-Izquierdo, D.J. Krebs, J.F. McGarry, R. Trunzo, A.-M. Novo-Gradac, J.L. Britt, J. Karsh, R.B. Katz, A.T. Lukemire, R. Szymkiewicz, D.L. Berry, J.P. Swinski, G.A. Neumann, M.T. Zuber, D.E. Smith, The Mercury laser altimeter instrument for the MESSENGER mission. *Space Sci. Rev.* **131**(1), 451–479 (2007)
- A.F. Cheng, O. Barnouin-Jha, M.T. Zuber, J. Veverka, D.E. Smith, G.A. Neumann, M. Robinson, P. Thomas, J.B. Garvin, S. Murchie, C. Chapman, L. Prockter, Laser altimetry of small-scale features on 433 Eros from NEAR-Shoemaker. *Science* **292**(5), 488–491 (2001)
- P.R. Christensen, V.E. Hamilton, G.L. Mehall, D. Pelham, W. O'Donnell, S. Anwar, H. Bowles, S. Chase, J. Fahlgren, Z. Farkas, T. Fisher, O. James, I. Kubik, I. Lazbin, M. Miner, M. Rassas, L. Schulze, K. Shamordola, T. Tourville, G. West, R. Woodward, D. Lauretta, The OSIRIS-REx thermal emission spectrometer (OTES) instrument. *Space Sci. Rev.* (2017, this issue)
- T.D. Cole, A.F. Cheng, R.A. Reiter, D.E. Smith, M.T. Zuber, Flight characterization of the NEAR Laser Rangefinder. *Proc. SPIE* **4035**, 131–142 (2000)

- D.S. Lauretta, A.E. Bartels, M.A. Barucci, E.B. Bierhaus, R.P. Binzel, W.F. Bottke, H. Campins, S.R. Chesley, B.C. Clark, B.E. Clark, E.A. Cloutis, H.C. Connolly, M.K. Crombie, M. Delbó, J.P. Dworkin, J.P. Emery, D.P. Glavin, V.E. Hamilton, C.W. Hergenrother, C.L. Johnson, L.P. Keller, P. Michel, M.C. Nolan, S.A. Sandford, D.J. Scheeres, A.A. Simon, B.M. Sutter, D. Vokrouhlický, K.J. Walsh, The OSIRIS-REx target asteroid (101955) Bennu: constraints on its physical, geological, and dynamical nature from astronomical observations. *Meteorit. Planet. Sci.* **50**(4), 834–849 (2015)
- D.S. Lauretta, S.S. Balram-Knutson, E. Beshore, W.V. Boynton, C.D. d'Aubigny, D.N. DellaGiustina, H.L. Enos, D.R. Gholish, C.W. Hergenrother, E.S. Howell, C.A. Johnson, E.T. Morton, M.C. Nolan, B. Rizk, H.L. Roper, A.E. Bartels, B.J. Bos, J.P. Dworkin, D.E. Highsmith, M.C. Moreau, D.A. Lorenz, L.F. Lim, R. Mink, J.A. Nuth, D.C. Reuter, A.A. Simon, E.B. Bierhaus, B.H. Bryan, R. Ballouz, O.S. Barnouin, R.P. Binzel, W.F. Bottke, V.E. Hamilton, K.J. Walsh, S.R. Chesley, P.R. Christensen, B.E. Clark, H.C. Connolly, M.K. Crombie, M.G. Daly, J.P. Emery, T.J. McCoy, J.W. McMahon, D.J. Scheeres, S. Messenger, K. Nakamura-Messenger, K. Righter, S.A. Sandford, OSIRIS-REx: sample return from Asteroid (101955) Bennu. *Space Sci. Rev.* (2017, this issue)
- S. Marchi, C.R. Chapman, O.S. Barnouin, J.E. Richardson, J.-B. Vincent, Cratering on asteroids, in *Asteroids IV*, ed. by P. Michel, F.E. DeMeo, W.F. Bottke (University of Arizona Press, Tucson, 2015), pp. 725–744
- J.W. McMahon, D.J. Scheeres, S.G. Hesar, D. Farnocchia, S. Chesley, D. Lauretta, The OSIRIS-REx radio science experiment at Bennu. *Space Sci. Rev.* (2017, this issue)
- H. Miyamoto, H. Yano, D.J. Scheeres, S. Abe, O. Barnouin-Jha, A.F. Cheng, H. Demura, R.W. Gaskell, N. Hirata, M. Ishiguro, T. Michikami, A.M. Nakamura, R. Nakamura, J. Saito, S. Sasaki, Regolith migration and sorting on asteroid Itokawa. *Science* **316**(5), 1011 (2007)
- T. Mizuno, T. Kase, T. Shiina, M. Mita, N. Namiki, H. Senshu, R. Yamada, H. Noda, H. Kunimori, N. Hirata, F. Terui, Y. Mimasu, Development of the laser altimeter (LIDAR) for Hayabusa 2. *Space Sci. Rev.* **208**(1–4), 1–15 (2017). doi:[10.1007/s11214-015-0231-2](https://doi.org/10.1007/s11214-015-0231-2)
- T. Mukai, H. Araki, T. Mizuno, N. Hatanaka, A.M. Nakamura, A. Kamei, H. Nakayama, A. Cheng, Detection of mass, shape and surface roughness of target asteroid of MUSES-C by LIDAR. *Adv. Space Res.* **29**(8), 1231–1235 (2002)
- M. Nimelman, J. Tripp, G. Bailak, J. Bolger, Spaceborne scanning lidar system (SSLS). *Proc. SPIE* **5798**, 73–82 (2005)
- M.C. Nolan, C. Magri, E.S. Howell, L.A. Benner, J.D. Giorgini, C.W. Hergenrother, R.S. Hudson, D.S. Lauretta, J.-L. Margot, S.J. Ostro, et al., Shape model and surface properties of the OSIRIS-REx target asteroid (101955) Bennu from radar and lightcurve observations. *Icarus* **226**(1), 629–640 (2013)
- S.C. Popescu, *Lidar Remote Sensing of Terrestrial Environments* (CRC Press, Boca Raton, 2012), p. 68
- D.C. Reuter, A.A. Simon, J. Hair, A. Lunsford, S. Manthripragada, V. Bly, B. Bos, C. Brambora, E. Caldwell, G. Casto, Z. Dolch, P. Finneran, D. Jennings, M. Jhabvala, E. Matson, M. McLelland, W. Roher, T. Sullivan, E. Weigle, Y. Wen, D. Wilson, D.S. Lauretta, The OSIRIS-REx visible and infrared spectrometer (OVIRS): spectral maps of the asteroid Bennu. *Space Sci. Rev.* (2017, this issue)
- B. Rizk, OCAMS: the OSIRIS-REx camera suite. *Space Sci. Rev.* (2017, this issue)
- D.J. Scheeres, S.G. Hesar, S. Tardivel, M. Hirabayashi, D. Farnocchia, J.W. McMahon, S.R. Chesley, O. Barnouin, R.P. Binzel, W.F. Bottke, M.G. Daly, J.P. Emery, C.W. Hergenrother, D.S. Lauretta, J.R. Marshall, P. Michel, M.C. Nolan, K.J. Walsh, The geophysical environment of Bennu. *Icarus* **276**, 116–140 (2016)
- D.E. Smith, M.T. Zuber, H.V. Frey, J.B. Garvin, J.W. Head, D.O. Muhleman, G.H. Pettengill, R.J. Phillips, S.C. Solomon, H.J. Zwally, W.B. Banerdt, T.C. Duxbury, M.P. Golombek, F.G. Lemoine, G.A. Neumann, D.D. Rowlands, O. Aharonson, P.G. Ford, A.B. Ivanov, C.L. Johnson, P.J. McGovern, J.B. Abshire, R.S. Afzal, X. Sun, Mars Orbiter Laser Altimeter: experiment summary after the first year of global mapping of Mars. *J. Geophys. Res.* **106**(E10), 23689–23722 (2001)
- D.E. Smith, M.T. Zuber, G.B. Jackson, J.F. Cavanaugh, G.A. Neumann, H. Riris, X. Sun, R.S. Zellar, C. Coltharp, J. Connelly, R.B. Katz, I. Kleyner, P. Liiva, A. Matuszeski, E.M. Mazarico, J.F. McGarry, A.-M. Novo-Gradac, M.N. Ott, C. Peters, L.A. Ramos-Izquierdo, L. Ramsey, D.D. Rowlands, S. Schmidt, V.S. Scott, G.B. Shaw, J.C. Smith, J.-P. Swinski, M.H. Torrence, G. Unger, A.W. Yu, T.W. Zagwodzki, The lunar orbiter laser altimeter investigation on the lunar reconnaissance orbiter mission. *Space Sci. Rev.* **150**, 209 (2010)
- D.E. Smith, M.T. Zuber, G.A. Neumann, E. Mazarico, F.G. Lemoine, J.W. Head III, P.G. Lucey, O. Aharonson, M.S. Robinson, X. Sun, M.H. Torrence, M.K. Barker, J. Oberst, T.C. Duxbury, D. Mao, O.S. Barnouin, K. Jha, D.D. Rowlands, S. Goossens, D. Baker, S. Bauer, P. Gläser, M. Lemelin, M. Rosenberg, M.M. Sori, J. Whitten, T. McClanahan, Summary of the results from the lunar orbiter laser altimeter after seven years in lunar orbit. *Icarus* **283**, 70–91 (2017)
- J. Whiteway, M. Daly, A. Carswell, T. Duck, C. Dickinson, L. Komguem, C. Cook, Lidar on the Phoenix mission to Mars. *J. Geophys. Res., Planets* **113**(E3), E00A08 (2008)